A&A 541, A124 (2012)
DOI: 10.1051/0004-6361/201117892

Astronomy & Astrophysics

The angular momentum transport by standard MRI in quasi-Kepler cylindrical Taylor-Couette flows

M. Gellert, G. Rüdiger, and M. Schultz

Leibniz-Institut für Astrophysik Potsdam, An der Sternwarte 16, 14482 Potsdam, Germany
e-mail: mgellert@aip.de

Received 16 August 2011 / Accepted 21 February 2012

ABSTRACT

We studied the instability of a dissipative quasi-Keplerian flow influenced by a homogeneous axial magnetic field in the geometry of a Taylor-Couette system. Especially we focus on the excitation of nonaxisymmetric modes and the resulting angular momentum transport, not on dynamo action. The excitation of nonaxisymmetric modes requires higher rotation rates than the excitation of the axisymmetric mode and this the more the higher the azimuthal mode number m is. We find that the weak-field branch in the instability map of the nonaxisymmetric modes always has a positive slope (in contrast to the axisymmetric modes) so that for given magnetic field the modes with $m > 0$ always have an upper limit of the supercritical Reynolds number. To excite a nonaxisymmetric mode at 1 AU in a Kepler disk, a minimum field strength of about 1 Gauss is necessary. For weaker magnetic field the nonaxisymmetric modes decay. The angular momentum transport of the nonaxisymmetric modes is always positive and depends linearly on the Lundquist number of the background field. The molecular viscosity and the basic rotation rate do not influence the related α-parameter. We did not find any indication that the magnetorotational instability decays for small magnetic Prandtl numbers as was found by using shearing-box codes. At 1 AU in a Kepler disk and with a field strength of about 1 Gauss α proves to be (only) about 0.005.

Key words. instabilities – magnetohydrodynamics (MHD)

1. Introduction

The long-standing problem of the generation of turbulence in various hydrodynamically stable situations has found a solution in recent years with the magnetohydrodynamic (MHD) shear flow instability, also called magnetorotational instability (MRI), in which the presence of a uniform axial magnetic field has a destabilizing effect on a differentially rotating flow with the angular velocity decreasing outward.

According to the Rayleigh criterion an ideal flow is stable against axisymmetric perturbations whenever the specific angular momentum increases outwards

$$\frac{\mathrm{d}}{\mathrm{d}R}\left(R^2\Omega\right)^2 > 0, \tag{1}$$

where (R, ϕ, z) are cylindrical coordinates, and Ω is the angular velocity. Kepler rotation with $\Omega \propto R^{-1.5}$ is therefore hydrodynamically stable against axisymmetric perturbations. It is not stable, however, under the presence of a uniform axial magnetic field (MRI). It is also not stable against nonaxisymmetric perturbations under the presence of a toroidal field (Azimuthal MRI). In these cases the stability condition (1) simplifies to

$$\frac{\mathrm{d}\Omega^2}{\mathrm{d}R} > 0. \tag{2}$$

For real fluids the instability condition looks more complicated. To be unstable, the rotation must be fast enough and the magnetic fields must not be too weak or too strong. The lower magnetic limit is fixed by the electric conductivity of the plasma, while the geometry of the disk determines the upper magnetic limit. We investigate in the following the lower limit through calculations. For numerical estimations we will use the values

$$\eta \simeq 4 \times 10^{15}\ \mathrm{cm}^2/\mathrm{s}, \qquad \rho \simeq 10^{-10}\ \mathrm{g/cm}^3, \tag{3}$$

(see Brandenburg & Subramanian 2005), for which we have derived a minimum field strength of 0.1 Gauss to excite unstable axisymmetric modes in the protoplanetary disk (Rüdiger & Kitchatinov 2005). This value is based on the calculation of the minimum magnetic Reynolds number

$$\mathrm{Rm}' = \frac{\Omega H^2}{\eta} \tag{4}$$

for fixed values of the half-thickness H of the disk and the magnetic Prandtl number

$$\mathrm{Pm} = \frac{\nu}{\eta}. \tag{5}$$

The vertical magnetic field B_z is measured in terms of the Lundquist number

$$\mathrm{S}' = \frac{B_z H}{\sqrt{\mu_0 \rho}\eta}, \tag{6}$$

for which Rm′ is the absolute minimum for given Pm. Note that in the definitions of Rm′ and S′ the molecular viscosity does not appear. The viscosity only appears in the definition of the magnetic Prandtl number (5).

The instability map $\mathrm{Rm}' = \mathrm{Rm}'(\mathrm{S}')$ for the *axisymmetric* mode and for fixed Pm is very characteristic. If a fixed Rm′ exceeds a minimum value of the order of 10, the instability exists between an upper limit and a lower limit of S′, which itself

must exceed a minimum value of the order of unity (see Fig. 2 in Rüdiger & Kitchatinov 2005). In the following the curve formed by the upper limits is called the strong-field branch and the curve formed by the lower limits is called the weak-field branch. The two branches have opposite slopes. For a given $S' \gtrsim 1$ there is only one value of Rm′ for marginal instability so that for *all* magnetic fields (above a lower limit) there is one rotation rate above which the axisymmetric MRI exists. For a certain $S'_{\rm min}$ the Rm′ takes its overall-minimum $Rm'_{\rm min}$. For all Pm between 10^{-4} and 10^3 the modes with the lowest Rm′ (which are easiest to excite) are axisymmetric.

The dependence of the curves of marginal stability on the magnetic Prandtl number Pm is only weak. For Pm < 1 there is no visible influence of Pm. Axisymmetric global MRI even exists for very small Pm with one and the same magnetic Reynolds number (but, of course, the ordinary Reynolds number takes very high values).

For Pm > 1 the behavior is different: both the critical $Rm'_{\rm min}$ and $S'_{\rm min}$ grow with $\sqrt{\rm Pm}$. Hence, the scaling for Pm > 1 switches to the parameters

$$\mathrm{Ha} = \frac{B_z H}{\sqrt{\mu_0 \rho \nu \eta}} \tag{7}$$

and

$$\mathrm{Rm}^* = \frac{\Omega H^2}{\sqrt{\nu\eta}} \tag{8}$$

(Kitchatinov & Rüdiger 2004). The critical rotation rate and magnetic field now run with $\sqrt{\nu\eta}$ instead of η, as it is true for Pm < 1. Both expressions are identical for Pm = 1. Again, the ratio of both quantities is free of the two dissipation parameters. The ratio of the linear rotation velocity and the Alfvén velocity of the vertical field is called the magnetic Mach number $\mathrm{Mm} = U_\phi / V_\mathrm{A}$ with

$$V_\mathrm{A} = \frac{B_z}{\sqrt{\mu_0 \rho}}. \tag{9}$$

At a distance of 1 AU and for a magnetic field of 1 Gauss, the magnetic Mach number is about 100. Because the possible magnetic field should be weaker than 1 Gauss, this value of Mm is certainly a *minimum*.

The behavior of the nonaxisymmetric modes is not so well known. We have learnt from the theory of the azimuthal magnetorotational instability (AMRI) that rotation that is too fast always destroys the instability. The AMRI follows from the interplay of differential rotation and a toroidal current-free magnetic field. It is basically nonaxisymmetric. For a given Lundquist number S there are two critical Reynolds numbers Rm. The instability is supercritical only between these two values of Rm. In other words, AMRI is excited by sufficiently fast rotation but it is suppressed by rotation that is too fast. The weak-field and the strong-field branch have the same positive slope in the plane Rm over S. The reason for this remarkable phenomenon is the smoothing influence of differential rotation on nonaxisymmetric magnetic perturbations.

The question arises whether the nonaxisymmetric modes of standard MRI are finally also supported by the differential rotation. The answer has consequences for i) possible dynamo models but also ii) for the magnetic field amplitudes necessary for the excitation of nonaxisymmetric modes. Let us assume for a moment that the weak-field branch of the instability map fulfills the condition

$$\mathrm{Rm} \simeq \mathrm{Mm}_{\rm weak}\, \mathrm{S}, \tag{10}$$

then

$$\frac{B_z}{\sqrt{\mu_0 \rho}} > \frac{U_\phi}{\mathrm{Mm}_{\rm weak}} \frac{H}{R} \tag{11}$$

for the minimum seed field B_z necessary for the excitation of the $m = 1$ mode. $\mathrm{Mm}_{\rm weak}$ is the (positive) slope of the curve according to the calculations. The result does not depend on the actual value of the magnetic diffusivity.

The same is true for the strong-field branches shown in Fig. 2. One finds the corresponding magnetic Mach number $\mathrm{Mm}_{\rm strong}$ much smaller than $\mathrm{Mm}_{\rm weak}$. For a given basic rotation the flow is unstable against nonaxisymmetric perturbations if

$$\mathrm{Mm}_{\rm strong} < \mathrm{Mm} < \mathrm{Mm}_{\rm weak}. \tag{12}$$

For Kepler disks the relation (11) can be read as

$$\beta \lesssim {\mathrm{Mm}_{\rm weak}}^2, \tag{13}$$

with $\beta = \mu_0 P / B_z^2$ as the plasma β. Hence, β must be quite small to excite nonaxisymmetric modes. The value of 400 used by Fromang et al. (2007) is so high that the corresponding magnetic fields could be much too weak to excite nonaxisymmetric instability modes. Kitchatinov & Rüdiger (2010) found the fairly moderate values $\mathrm{Mm}_{\rm strong} \simeq 2$ and $\mathrm{Mm}_{\rm weak} \simeq 10$ for a simplified Kepler disk. For these low values the unstable domain of the nonaxisymmetric modes is quite restricted. We find that the numerical values of the critical magnetic Mach numbers for the weak-field branch for modes in infinite cylinders are much higher.

2. The model

The MRI has been found by considering the stability problem of Taylor-Couette (TC) flows of magnetized ideal fluids by Velikhov (1959). Because of the simplicity of this geometry, much work has been done to study the MRI for fluids between cylinders rotating with different angular velocities. Theory (Rüdiger & Zhang 2001; Ji et al. 2001) and experiments (see Stefani et al. 2009) revealed the possibilities to realize the MRI even in the laboratory.

In the following, two concentric cylinders (unbounded in z) of radii $R_{\rm in}$ and $R_{\rm out}$ are considered with the rotation rates $\Omega_{\rm in}$ and $\Omega_{\rm out}$. The rotation profile between the cylinders may mimic the Kepler rotation law, i.e. we fix $\Omega_{\rm out} = 0.35\Omega_{\rm in}$. The value ensures that the cylinders with $R_{\rm out} = 2R_{\rm in}$ rotate like planets. We call this radial rotation profile quasi-Keplerian profile.

The boundaries are assumed to be impenetrable, stress-free and perfectly conducting, which is valid also for almost all liquid metal experiments in the laboratory. The cylinders are infinite in the axial direction. Fricke (1969) and Balbus & Hawley (1990) were the first to apply the instability to important astrophysical applications. To be closer to the physics of accretion disks, we also considered a pseudo-vacuum condition for the outer boundary in the nonlinear simulations.

The governing equations are

$$\frac{\partial \boldsymbol{u}}{\partial t} + (\boldsymbol{u}\nabla)\boldsymbol{u} = -\frac{1}{\rho}\nabla P + \nu\Delta\boldsymbol{u} + \frac{1}{\mu_0}\mathrm{curl}\,\boldsymbol{B}\times\boldsymbol{B}, \tag{14}$$

$$\frac{\partial \boldsymbol{B}}{\partial t} = \mathrm{curl}(\boldsymbol{u}\times\boldsymbol{B}) + \eta\Delta\boldsymbol{B}, \tag{15}$$

and

$$\mathrm{div}\,\boldsymbol{u} = \mathrm{div}\,\boldsymbol{B} = 0, \tag{16}$$

where $\boldsymbol{u}$ is the velocity, $\boldsymbol{B}$ the magnetic field, P the pressure, ν the kinematic viscosity, and η the magnetic diffusivity.

The basic state is $u_R = u_z = B_R = B_\phi = 0$, $B_z = B_0 =$ const. and

$$U_\phi = R\Omega = aR + \frac{b}{R}, \tag{17}$$

where a and b are constants defined by

$$a = \Omega_{\rm in}\frac{\mu_\Omega - \hat\eta^2}{1-\hat\eta^2}, \quad b = \Omega_{\rm in}R_{\rm in}^2\frac{1-\mu_\Omega}{1-\hat\eta^2}, \tag{18}$$

with

$$\hat\eta = \frac{R_{\rm in}}{R_{\rm out}}, \qquad \mu_\Omega = \frac{\Omega_{\rm out}}{\Omega_{\rm in}}. \tag{19}$$

The axial field amplitude is now measured by the Hartmann number

$$\mathrm{Ha} = \frac{B_0 D}{\sqrt{\mu_0\rho\nu\eta}}. \tag{20}$$

$D = R_{\rm out} - R_{\rm in}$ is used as the unit of length, ν/D as the unit of velocity. The rotation Ω is normalized with the inner rotation rate $\Omega_{\rm in}$. The magnetic Reynolds number Rm is defined as

$$\mathrm{Rm} = \frac{\Omega_{\rm in}D^2}{\eta}. \tag{21}$$

The Lundquist number S is defined by $\mathrm{S} = \mathrm{Ha}\cdot\sqrt{\mathrm{Pm}}$. Expressed with the Alfvén frequency $\Omega_{\rm A}$ it is

$$\frac{\Omega_{\rm A}}{\Omega_{\rm in}} = \frac{\mathrm{S}}{\mathrm{Rm}}. \tag{22}$$

All calculations in this paper were made for a model with $\hat\eta = 0.5$. This is the only geometry where the scales $R_{\rm in}$ and D are equal. As the magnetic Mach number we used the quantity $\mathrm{Mm} = \Omega_{\rm in}/\Omega_{\rm A}$.

3. Wave number and drift frequencies

Equations (14)–(16) are linearized with respect to the background state (17). The perturbed quantities are developed after azimuthal Fourier modes

$$F = F(R)\mathrm{e}^{\mathrm{i}(kz+m\phi+\omega t)}. \tag{23}$$

The results are optimized in the wave number k. Only the solutions with those k are of interest where the Reynolds numbers take a minimum. All solutions with another k have higher Reynolds numbers. One can also show that the solutions with a certain positive k are always accompanied by a solution with $-k$ but with the same Reynolds number and drift frequency (for given Ha and m). Because the pitch angle of the resulting spirals is given by $B_z/B_\phi \propto -m/k$, it is clear that both solutions have opposite pitch angles so that the solution is always a combination of a left-handed and a right-handed screw.

The proof is as follows. After eliminating the pressure fluctuations and the fluctuations of the vertical magnetic field, B_z', using Eq. (16), the linearized equations are

$$\frac{\partial u_R}{\partial R} + \frac{u_R}{R} + \frac{\mathrm{i}m}{R}u_\phi + \mathrm{i}ku_z = 0, \tag{24}$$

$$\begin{aligned}
&\frac{\partial^2 u_\phi}{\partial R^2} + \frac{1}{R}\frac{\partial u_\phi}{\partial R} - \frac{u_\phi}{R^2} - \left(\frac{m^2}{R^2}+k^2\right)u_\phi \\
&-\mathrm{i}\left(m\mathrm{Re}\frac{\Omega}{\Omega_{\rm in}}+\omega\right)u_\phi + \frac{2\mathrm{i}m}{R^2}u_R - \mathrm{Re}\frac{1}{R}\frac{\partial}{\partial R}\left(R^2\frac{\Omega}{\Omega_{\rm in}}\right)u_R \\
&-\frac{m}{k}\left[\frac{1}{R}\frac{\partial^2 u_z}{\partial R^2} + \frac{1}{R^2}\frac{\partial u_z}{\partial R} - \left(\frac{m^2}{R^2}+k^2\right)\frac{u_z}{R}\right. \\
&\left.-\mathrm{i}\left(m\mathrm{Re}\frac{\Omega}{\Omega_{\rm in}}+\omega\right)\frac{u_z}{R}\right] + \frac{m}{k}\mathrm{Ha}^2\left[\frac{1}{R}\frac{\partial B_R}{\partial R} + \frac{B_R}{R^2}\right] \\
&+\frac{\mathrm{i}}{k}\mathrm{Ha}^2\left(\frac{m^2}{R^2}+k^2\right)B_\phi = 0,
\end{aligned} \tag{25}$$

$$\begin{aligned}
&\frac{\partial^3 u_z}{\partial R^3} + \frac{1}{R}\frac{\partial^2 u_z}{\partial R^2} - \frac{1}{R^2}\frac{\partial u_z}{\partial R} - \left(\frac{m^2}{R^2}+k^2\right)\frac{\partial u_z}{\partial R} \\
&+\frac{2m^2}{R^3}u_z - \mathrm{i}\left(m\mathrm{Re}\frac{\Omega}{\Omega_{\rm in}}+\omega\right)\frac{\partial u_z}{\partial R} - \mathrm{i}m\mathrm{Re}\frac{\partial}{\partial R}\left(\frac{\Omega}{\Omega_{\rm in}}\right)u_z \\
&-\mathrm{Ha}^2\left[\frac{\partial^2 B_R}{\partial R^2} + \frac{1}{R}\frac{\partial B_R}{\partial R} - \frac{B_R}{R^2} - k^2 B_R\right. \\
&\left.+\frac{\mathrm{i}m}{R}\frac{\partial B_\phi}{\partial R} - \frac{\mathrm{i}m}{R^2}B_\phi\right] - \mathrm{i}k\left[\frac{\partial^2 u_R}{\partial R^2} + \frac{1}{R}\frac{\partial u_R}{\partial R} - \frac{u_R}{R^2}\right. \\
&\left.-\left(k^2+\frac{m^2}{R^2}\right)u_R\right] - k\left(m\mathrm{Re}\frac{\Omega}{\Omega_{\rm in}}+\omega\right)u_R \\
&-2\frac{km}{R^2}u_\phi - 2\mathrm{i}k\mathrm{Re}\frac{\Omega}{\Omega_{\rm in}}u_\phi = 0,
\end{aligned} \tag{26}$$

$$\begin{aligned}
&\frac{\partial^2 B_R}{\partial R^2} + \frac{1}{R}\frac{\partial B_R}{\partial R} - \frac{B_R}{R^2} - \left(\frac{m^2}{R^2}+k^2\right)B_R \\
&-\frac{2\mathrm{i}m}{R^2}B_\phi - \mathrm{i}\mathrm{Pm}\left(m\mathrm{Re}\frac{\Omega}{\Omega_{\rm in}}+\omega\right)B_R + \mathrm{i}ku_R = 0,
\end{aligned} \tag{27}$$

$$\begin{aligned}
&\frac{\partial^2 B_\phi}{\partial R^2} + \frac{1}{R}\frac{\partial B_\phi}{\partial R} - \frac{B_\phi}{R^2} - \left(\frac{m^2}{R^2}+k^2\right)B_\phi \\
&+\frac{2\mathrm{i}m}{R^2}B_R - \mathrm{i}\mathrm{Pm}\left(m\mathrm{Re}\frac{\Omega}{\Omega_{\rm in}}+\omega\right)B_\phi + \mathrm{i}ku_\phi \\
&+\mathrm{Pm}\ \mathrm{Re}\,R\frac{\partial\Omega/\Omega_{\rm in}}{\partial R}B_R = 0
\end{aligned} \tag{28}$$

(Shalybkov et al. 2002). The eigenfrequency ω is here normalized with the viscosity frequency ν/R_0^2. One finds the system invariant against the simultaneous transformation $k \to -k$, $u_z \to -u_z$, $B_R \to -B_R$ and $B_\phi \to -B_\phi$. Hence, if a solution is known for a certain k, then a modified solution always exists for $-k$. The standard MRI in cylindric geometry always produces the same number of left and right screws[1]. The total helicity (kinetic and magnetic) is thus vanishing (Fig. 1).

Conjugating the linearized equation system (24)–(28) we find that the system is invariant against the simultaneous transformations $m \to -m$, $k \to -k$ and $\Re(\omega) \to -\Re(\omega)$. Hence, both the pattern drift $\partial\phi/\partial t = -\Re(\omega)/m$ of both solutions as well as the pitch

$$\frac{\partial z}{\partial\phi} = -\frac{m}{k} \tag{29}$$

are equal so that the two solutions are identical. It is therefore sufficient to consider the solutions for positive m.

[1] The same is true for the instability of toroidal fields between the cylinders with and without electric current, see Rüdiger et al. (2011).

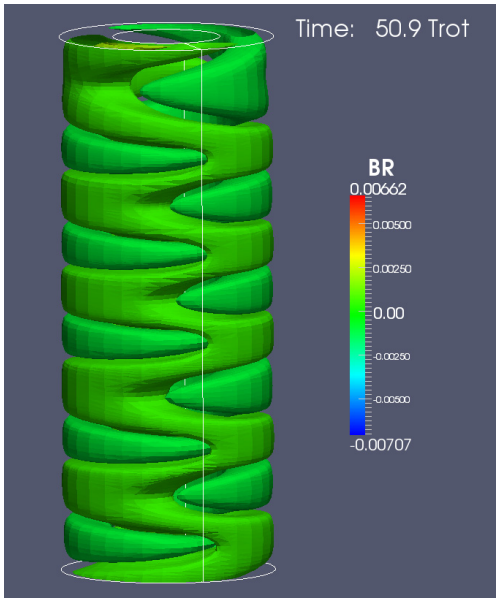

Fig. 1. Simultaneous existence of the two modes with k and $-k$ in the nonlinear regime. The whole pattern drifts in the direction of rotation. Rm = 160, S = 13, Pm = 1.

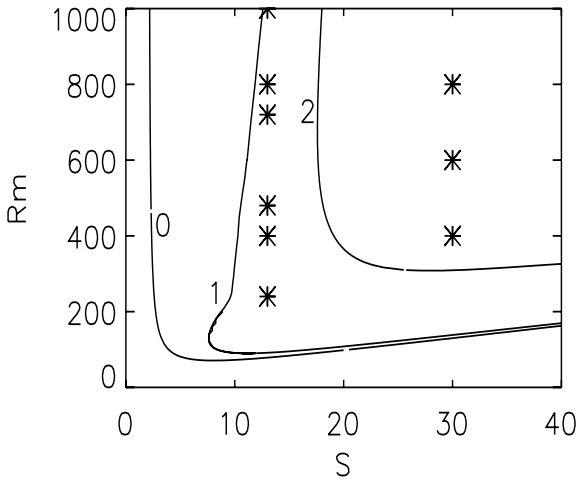

Fig. 2. Instability map of the modes with $m = 0$, $m = 1$ and $m = 2$ in quasi-Kepler flows ($\mu_\Omega = 0.35$). For a given Rm the flow is unstable for Lundquist numbers S between the values at the weak-field branch and the strong-field branch. Star symbols mark the series of nonlinear simulations discussed below. Pm = 1.

The unstable Taylor-Couette flow forms axisymmetric or nonaxisymmetric vortices. With our normalization the vertical extent δz of a vortex is given by

$$\frac{\delta z}{R_{\rm out} - R_{\rm in}} = \frac{\pi}{k}\sqrt{\frac{\hat{\eta}}{1-\hat{\eta}}}, \tag{30}$$

hence for $\hat{\eta} = 0.5$

$$\frac{\delta z}{R_{\rm out} - R_{\rm in}} = \frac{\pi}{k}. \tag{31}$$

For $k \simeq \pi$ the cells have the same vertical extent as they have in radius, and for $k \gg \pi$ the cells are very flat. Generally, the vortices of the axisymmetric modes become more and more elongated in the vertical direction, $k \ll \pi$.

The drift velocity $\mathcal{R}(\omega)$ always proved to be negative, i.e., the pattern drifts are in the direction of the rotation (eastward). It is

$$\dot{\phi} = -\frac{\mathcal{R}(\omega)\Omega_{\rm in}}{m}, \tag{32}$$

so that the eastern drift period in units of the rotation period is $m/\mathcal{R}(\omega)$. Note that we are working in the resting laboratory system.

4. Solutions for Pm = 1

We start with the standard case Pm = 1 where there is no difference either between the two Reynolds numbers or between the Hartmann number and the Lundquist number. Most numerical simulations are conducted with these parameters. The critical Reynolds numbers for the excitation of the modes with $m = 0$, $m = 1$ and $m = 2$ in quasi-Kepler flows are given in Fig. 2.

For the given Lundquist numbers the Reynolds numbers are minimized by varying the axial wave number k. Note the existence of an absolute minimum $\mathrm{Re}_{\rm MIN}$ of the Reynolds number. It is smaller for the axisymmetric mode than for the nonaxisymmetric modes. The nonaxisymmetric modes need faster rotation for their excitation. There is a basic difference, however, between the axisymmetric and the nonaxisymmetric modes. For $m = 0$ and $\mathrm{S} \simeq 1$ there is always *one* critical Reynolds number above which the MRI is excited for *all* larger Rm. The absolute minimum value for S is of the order of unity. On the other hand, the critical Lundquist values for the nonaxisymmetric modes with $m > 0$ behave completely different. For $\mathrm{S} > \mathrm{S}_{\rm MIN}$, where $\mathrm{S}_{\rm MIN} \simeq 1$ is the smallest possible Lundquist number, there are always *two* critical Reynolds numbers between which the nonaxisymmetric MRI modes can exist (Fig. 2). Hence, the nonaxisymmetric mode cannot survive if the rotation is too fast. The differential rotation excites the MRI but – if it is too strong – it suppresses its nonaxisymmetric parts.

The rotational quenching of the nonaxisymmetric parts of the MRI should have serious consequences for the dynamo problem. Following the theorem by Cowling, all dynamo models need nonaxisymmetric parts of the magnetic field.

The $m = 1$ mode in Fig. 2 needs seed fields that are the higher the faster the rotation. As an estimate one finds

$$\Omega_{\rm A} \simeq 3 \times 10^{-3}\ \Omega_{\rm in} \tag{33}$$

($\mathrm{Mm}_{\rm weak} \simeq 320$). If we assume the linear velocity of the Kepler disk at 1 AU to be faster than 30 $\mathrm{km\,s^{-1}}$ (solar system) and the density at this place to be 10^{-10} $\mathrm{g/cm^3}$, then the relation (33) means

$$B_0 > 1 \ \text{Gauss}, \tag{34}$$

which is a very high value at the distance. The value (34) is needed to start any MRI-dynamo. It exceeds the above mentioned minimum value of 0.1 Gauss for the excitation of axisymmetric modes by one order of magnitude. The very high value of this field strength suggests that the weak-field branch of the MRI bifurcation map is indeed the branch of astrophysical relevance and not the strong-field branch. For the latter one finds $\Omega_{\rm A} \simeq 0.3\ \Omega_{\rm in}$, representing magnetic fields that are by a factor of hundred (!) stronger than the fields at the weak-field branch. It is hard to imagine that such fields are available for the formation of protoplanetary disks.

The results for the wave numbers (for which the Reynolds numbers for fixed S are minimum) are plotted in Fig. 3 (left).

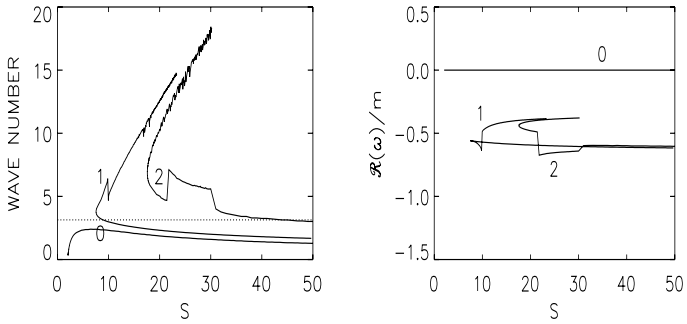

Fig. 3. Same as in Fig. 2 but for the normalized wave number (*left*) and the drift frequency (*right*).

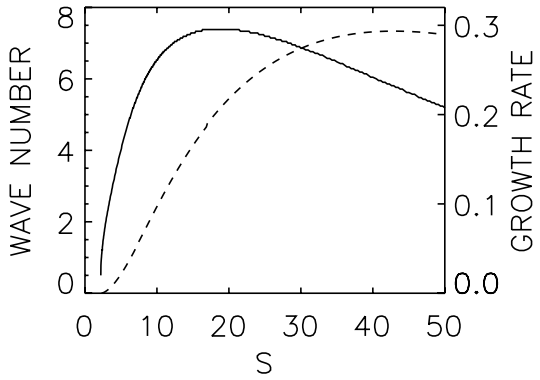

Fig. 4. Dependence on the magnetic field of the wave number of the axisymmetric mode and the growth rate (dashed) for given Reynolds number Rm = 500. $m = 0$, Pm = 1.

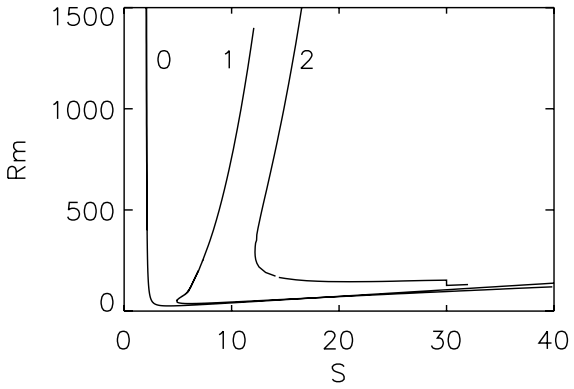

Fig. 5. Same as in Fig. 2 but for Pm = 0.01. At the strong-field branch for S > 20 the nonaxisymmetric mode becomes the mode with the lowest magnetic Reynolds number.

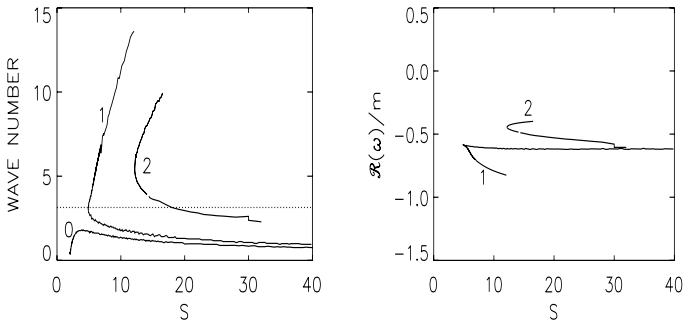

Fig. 6. Normalized wave number (*left*) and drift frequency (*right*) for Pm = 0.01.

The dotted line gives $k = \pi$, for which the cells after (31) are nearly spherical. For $k < \pi$ the cells tend to be prolate, while they are oblate for $k > \pi$. This is, of course, only true if the radial cell size is of the order of the distance between the cylinders, which must be checked as well.

There are surprising differences in Fig. 3 (left) for axisymmetric and nonaxisymmetric modes. All axisymmetric rolls are prolate, their axial size exceeds the radial scale. This is true for all values of the magnetic field. The result is not surprising because magnetic fields always increase the correlation length along the field, hence for strong fields we have $k \propto 1/\mathrm{S}$. That for $m = 0$ the wave numbers k for given Rm are small at the weak-field (left) branch as well as at the strong-field (right) branch of the marginal instability curve does *not* mean that they are small also in between. Kitchatinov & Rüdiger (2004) found the relation $k \simeq V_\mathrm{A}/\eta$ with a local approximation close to the left branch that the wave number runs with S. One must consequently expect that between the left and right branch there is a maximum of k so that there the axisymmetric modes also have short axial scales – as we demonstrate in Fig. 8 (top, right). Figure 4 gives for Rm = 500 the mentioned maximum of the axial wave number together with the growth rate. One finds that the axisymmetric channel mode forms thin rolls only close to the left branch, but the rolls are thick for stronger fields, i.e., values of $\mathrm{Mm} \gtrsim 1$.

For $m = 1$ only the cells with large S are almost rolls. The wave numbers for both branches are quite different. They are large for the weak-field branch and small for the strong-field branch. The cells for the marginal modes along the weak-field branch are therefore fairly flat. This is only true, however, if the radial eigenfunctions smoothly cover the distance between the cylinders.

The drift of the nonaxisymmetric modes is eastward typically 50% of the rotation frequency of the inner cylinder, i.e., the MRI pattern drift is westward with respect to the rotating system. because the outer cylinder only rotates with 35% of the rotation frequency, the field pattern rotates by 42% faster than the outer cylinder. The corotation radius of the MRI pattern is located between the two cylinders close to the middle between the cylinders. The same is true, at least qualitatively, for the pattern with $m = 2$. A test calculation with $\hat{\eta} = 0.8$ leads to a pattern drift $-\Re(\omega)/m \simeq 0.85$, which also yields a corotation radius just in the middle of the two cylinders.

5. Solutions for Pm = 0.01

The results for smaller magnetic Prandtl numbers (Pm = 0.01) are given in plots 5 and 6. In the weak-field limit the differences to Pm = 1 are quite small. The rotational quenching of the nonaxisymmetric modes seems to be slightly weaker than for larger Pm ($\mathrm{Mm}_\mathrm{weak} \simeq 400$).

The behavior of the wave number and the azimuthal drift is also fairly obvious. The cells in the weak-field limit are flat, while they are highly aligned along the rotation axis in the strong-field limit (Fig. 6, left). The axisymmetric cells are longer than the nonaxisymmetric cells.

More striking is the phenomenon for strong fields for which the marginal-stability curves for $m = 0$ and $m = 1$ cross near $\mathrm{S} \simeq 18$. The mode with the global minimum Reynolds number

is always axisymmetric, but for stronger magnetic fields the critical Reynolds numbers for $m = 1$ are smaller than those for $m = 0$. For these fields and for increasing Reynolds numbers MRI sets in as a nonaxisymmetric flow pattern. The nonaxisymmetric structure is lost, however, for rotation that is too fast when the magnetic Reynolds number reaches the upper value of the marginal instability of the $m = 1$ mode and the solution becomes axisymmetric again. We have found this sort of mode crossing for different geometries (Kitchatinov & Rüdiger 1997) as well as with different codes (Shalybkov et al. 2002). So far this phenomenon is only known for MHD flows between conducting cylinders.

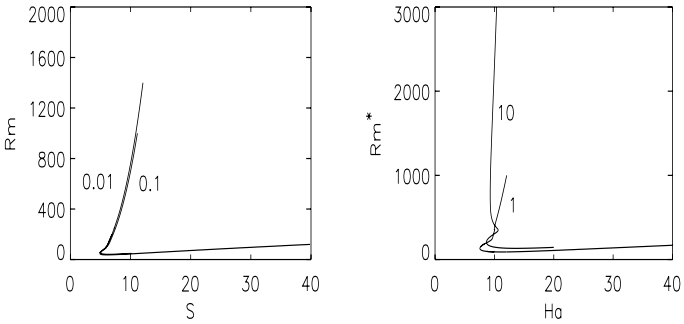

Fig. 7. Critical Reynolds numbers for the nonaxisymmetric modes with $m = 1$ for small (*left*) and large (*right*) magnetic Prandtl numbers.

6. The magnetic Prandtl number dependence

There are simple scaling laws for the marginal instability. They appear if the instability domains for large magnetic Prandtl numbers are also computed. The results for Pm = 10 are plotted with the variable Rm^* and Ha (Fig. 7, right). Figures 7 demonstrate the small differences of the curves for small Pm if scaled with Rm and S, while the same is true for the curves for large Pm if scaled with Rm^* and Ha. In both cases the ratio of the characteristic numbers is the magnetic Mach number, which is free of any diffusivity values. We find a somewhat weaker rotational quenching

$$\Omega_\mathrm{A} \simeq 3 \times 10^{-4}\, \Omega_\mathrm{in} \tag{35}$$

of the nonaxisymmetric modes for Pm > 1 compared with the relation (33), which holds for Pm $\leq$ 1. Generally the weak-field edges of the instability domains for Pm $\lesssim$ 1 show a positive slope. However, after inspecting Fig. 7 (right) for Pm = 10, the slope is very steep and it is unclear whether it is still positive. In any case, the behavior of the weak-field limit for large Prandtl numbers slightly differs from that of the curves for smaller Pm. The differences provided by the strong-field branches are very small for the two regimes.

7. Nonlinear simulations

With the 3D spectral MHD code for cylindric geometry described by Gellert et al. (2007) nonlinear simulations of global MRI are possible. The code works with M Fourier modes in the azimuthal direction, a typical value used in the calculations is $M = 16$ for the fairly narrow spectrum of excited modes.

7.1. The instability pattern

The simulations concerning the instability pattern are related to the map of marginal instability for Pm = 1 (Fig. 2) for a fixed Lundquist number S = 13. Three examples are given. The first works with relatively slow rotation, while the second container rotates faster or much faster. The marginal instability appears for a minimum magnetic Mach number of about 6. The first model lies below the instability domain of $m = 1$, the second one inside the $m = 1$ domain, and the third model lies outside. The magnetic Mach numbers for the considered cases are Mm = 7, Mm = 46 and Mm = 96.

The nonlinear calculations are important because our curves for marginal instability of nonaxisymmetric modes only concern the stability behavior of the Kepler flow under the presence of the axial field. It is also possible that the rolls of the $m = 0$ solution become unstable against disturbances with $m > 0$, leading to secondary instabilities with nonaxisymmetric patterns.

Figure 8 shows the results. For a given magnetic field amplitude (S = 13) simulations with Rm = 88, Rm = 600, and one with Rm = 1250 are presented. Only the value Rm = 600 lies in the instability map (Fig. 2) between the lower and the upper limit for nonaxisymmetric instability and only in this case a nonaxisymmetric (drifting) magnetic pattern results (8, middle). From the beginning, the mode with $m = 0$ grows fastest and the mode with $m = 1$ also grows continuously. The other modes come much later so that the complete pattern occurs only after 30 orbits.

The opposite is true for faster rotation (Fig. 8, right). Here only the mode with $m = 0$ grows, while all the nonaxisymmetric modes decay (Fig. 8, bottom right). The resulting magnetic pattern is axisymmetric despite the high value of the Reynolds number. Clearly, therefore, the linear approximation provides the real instability behavior. For the considered rotation rates a nonaxisymmetric instability of the magnetic $m = 0$ pattern does not appear in the numerical simulations.

Note that – as predicted by the linear results for the axial wave numbers (Fig. 3, left) – the axisymmetric cells for Reynolds numbers close to the instability limit are indeed prolate (Fig. 8, left). They do become oblate for the fast-rotation case (Fig. 8, right) despite the action of the Taylor-Proudman theorem. The nonaxisymmetric modes form a spectrum of modes (see Fig. 8, middle). Only models of this kind are used in the next section to compute the outward angular momentum transport of the MRI. Only for these models the equations form a nonlinear mixture of many azimuthal modes close to the transition of turbulence. Obviously, rotation that is too fast destroys the resulting mixture (Fig. 8, bottom right).

The amplitudes of the MRI-induced magnetic fluctuations are also important. They easily exceed the strength of the axial background field, but only in the domain where the nonaxisymmetric modes are excited (see Fig. 8). On the other hand, the amplitudes of the toroidal field components grow with growing Reynolds number. For Re = 600 the maximum B_ϕ exceeds the axial background field by one order of magnitude.

7.2. The angular momentum transport

The total angular momentum transport in radial direction is

$$T_{R\phi} = \langle u_R' u_\phi' \rangle - \frac{1}{\mu_0 \rho} \langle B_R' B_\phi' \rangle, \tag{36}$$

which in the usual manner can be written as

$$T_{R\phi} = -\nu_\mathrm{T} R \frac{\mathrm{d}\Omega}{\mathrm{d}R} = \alpha_\mathrm{SS} \Omega^2 D^2, \tag{37}$$

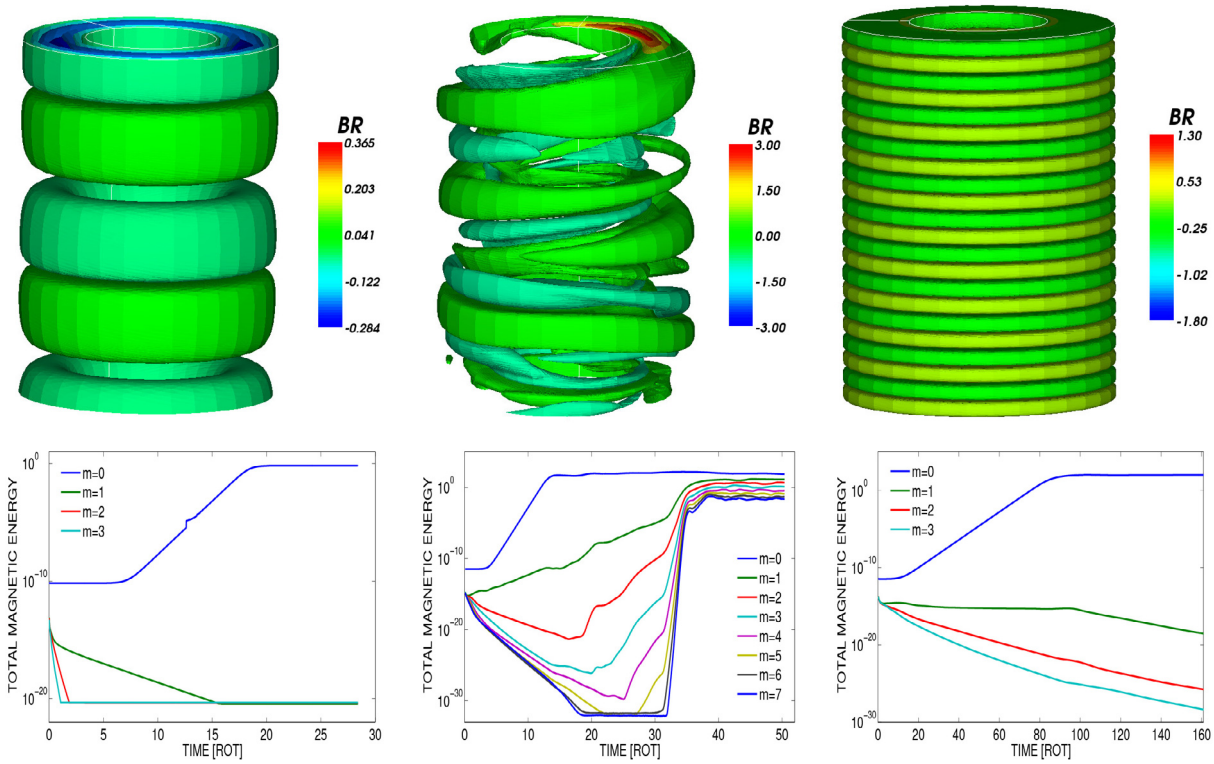

Fig. 8. *Top*: radial component of the magnetic field for S = 13 and for slow rotation (Rm = 88, *left*), medium rotation (Rm = 600, *middle*) and fast rotation (Rm = 1250, *right*). For slow and for fast rotation the nonlinear instability pattern is purely axisymmetric and for medium rotation it is nonaxisymmetric. *Bottom*: the same for the energies in the Fourier modes of the magnetic field. Pm = 1.

with D as the gap width of the container. Hence, the MRI-α as the normalized angular momentum transport can be computed with the definition

$$\alpha_{\rm SS} = \frac{T_{R\phi}}{\Omega^2 D^2}. \tag{38}$$

Note that this definition differs from the usual one unless $D \simeq H$, which values are indeed of the same order for thick disks. In the first step we computed the quantity (38) by averaging only over the azimuth (Fig. 9). One learns that the angular momentum transport is positive everywhere with a weak indication of the cell structure. There are no areas in the computational domain with negative angular momentum transport. Generally, according to our experiences, the Maxwell part in the relation (36) dominates the Reynolds term.

To overcome the axial inhomogeneity, we continued to average over the z coordinate so that the resulting expression remains only a function of R. The resulting profile shows a characteristic maximum because it must vanish at the boundaries because of the boundary conditions. The question is how this maximum is related to the mean pressure in the computational domain. The pressure in the container vanishes at the inner cylinder and monotonously grows toward the outer cylinder. The radially averaged pressure for Kepler rotation between the bounding cylinders is of the order of $\rho\Omega^2 D^2$ so that indeed the relation (37) can be read as

$$\rho T_{R\phi} = \alpha_{\rm SS}\ p. \tag{39}$$

This is the standard relation of the accretion theory, which – as we now know – only holds in the model after averaging over the entire cylinder.

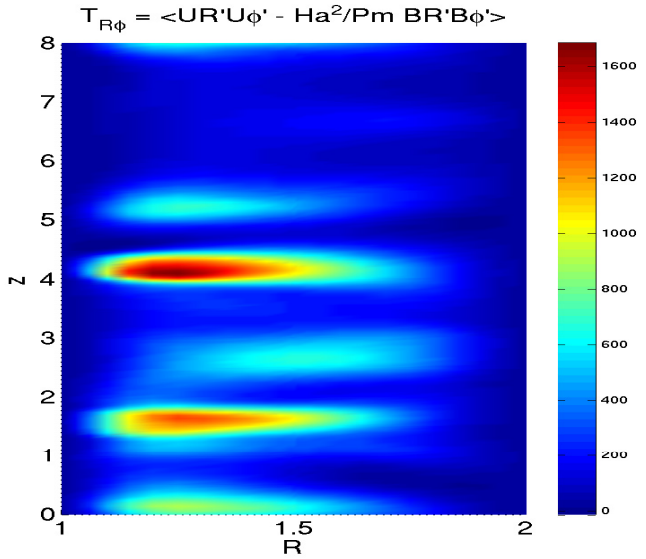

Fig. 9. Angular momentum transport parameter α if averaged only over the azimuth is positive everywhere and only slightly reflecting a cell structure. Rm = 400, S = 30, Pm = 1.

In the next step, therefore, the averaging procedure concerns the full container. The following results for the $\alpha_{\rm SS}$ parameter only concern this model. They are given in Fig. 10, and can be represented by the *linear* relation

$$\alpha_{\rm SS} = 4.8 \times 10^{-5}\ {\rm S}, \tag{40}$$

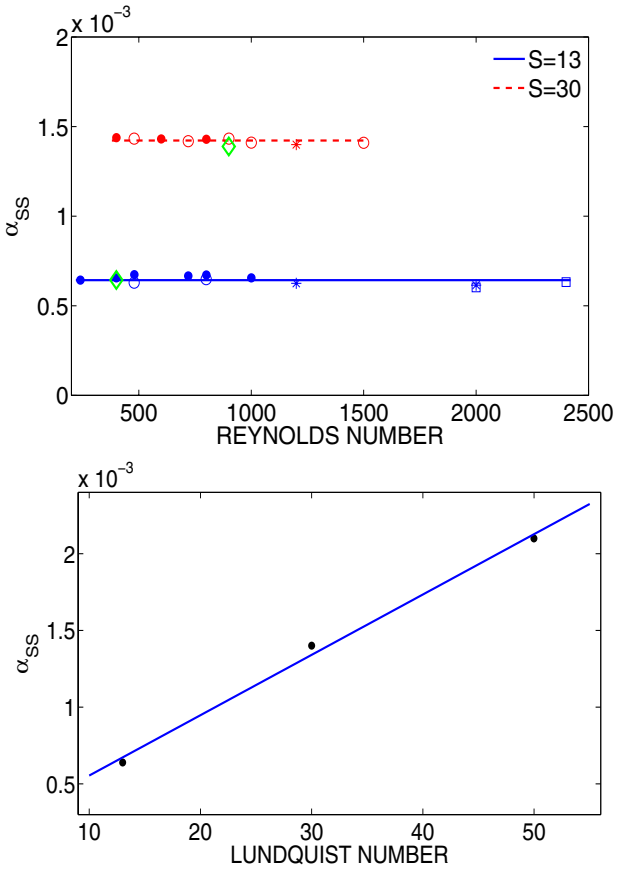

Fig. 10. Normalized angular momentum transport α_{SS} (averaged over the entire cylinder) in its dependence on the Reynolds number (*top*) and the Lundquist number S (*bottom*). Influences of the viscosity and the basic rotation on the angular momentum transport parameter α_{SS} do not appear. Dots: Pm = 1.0, circles: Pm = 0.5, stars: Pm = 0.2, square: Pm = 0.1. Green diamonds: Pm = 1.0 and pseudo-vacuum as outer boundary condition.

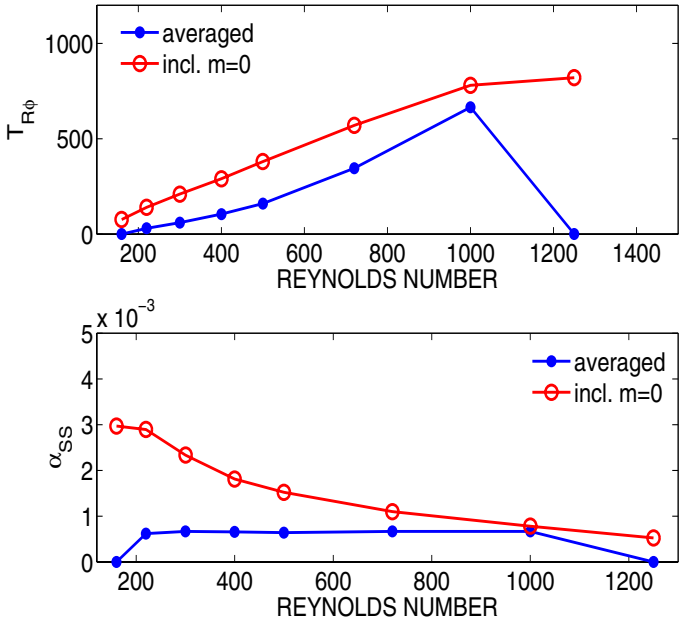

Fig. 11. Normalized angular momentum transport α_{SS} (averaged over the entire cylinder) in its dependence on the Reynolds number. Open circles represent the values if the contribution of the channel mode ($m = 0$) is added. S = 13, Pm = 1.

valid for all considered Reynolds numbers and magnetic Prandtl numbers (Pm $\leq$ 1) given in Fig. 2 with star symbols. There is no dependence of the α_{SS} on the rotation rate unless the chosen value of the magnetic Reynolds number lies too close to the boundaries of the instability map (Fig. 2). For two examples for Pm = 1 (green diamonds in Fig. 10) the outer boundary condition has been changed from perfect conductor to pseudo-vacuum. The numbers do not show a remarkable influence of the boundary conditions on the resulting values of α_{SS}. Apparently shearing box simulations give a stronger dependence on the magnetic field with $\alpha_{SS} \propto B^2$ (Brandenburg et al. 1996). The reason is not obvious.

From Eq. (40) one finds with the numbers (3) that

$$\alpha_{SS} \simeq 0.005 \frac{B}{1\ \mathrm{Gauss}} \frac{D}{1\ \mathrm{AU}}. \quad (41)$$

Hence, the numerical value of the MRI-α linearly depends on the amplitude of the magnetic field and/or the size of the disk or the torus. According to definition (37), one can also understand our α_{SS} as a realization of the β viscosity in the sense of Duschl et al. (2000) and Huré et al. (2001). Obviously the magnetic field amplitude must be not much lower than about one Gauss to obtain α_{SS} values of about 0.01 or even higher.

The angular momentum transport shown in Fig. 10 is only due to the nonaxisymmetric modes with $m > 0$. Only these modes have been defined as the "fluctuations" in the definitions of the random functions $\boldsymbol{u}$ and $\boldsymbol{B}$ and the well-defined averaging procedure is considered as the integration over ϕ. We have shown in Fig. 8 that only these modes in our simulations are coming close to develop turbulence.

The question remains whether also the axisymmetric modes with $m = 0$ contribute to the angular momentum transport. They can be defined as fluctuations only by their small-scale spatial vertical variations, which are characterized by the vertical wave number k. Then the basic rotation can only be defined by $\langle u_\phi \rangle$ after averaging over z. The fluctuations of the flow and the field defined in this way do indeed transport angular momentum. If the axisymmetric modes are also used for the calculation of the angular momentum, the resulting values always lie above the curves for the nonaxisymmetric modes (Figs. 11 and 12). For higher Reynolds numbers the extra value by the axisymmetric modes diminishes so that the lines in the Figs. 11 and 12 are approaching. In this picture the relation (40) remains true if the Reynolds numbers are large enough compared to the Lundquist number S, i.e., in the regime of high magnetic Mach number. With these high values of the magnetic Mach number as discussed above the contributions of the axisymmetric modes to the viscosity-α indeed remain small.

We show in Fig. 11 that the angular momentum transport by the nonaxisymmetric modes stops for Rm $\simeq$ 1200. For larger Reynolds numbers the axisymmetric rolls shown in Fig. 8 (top, right) alone produce the viscosity-α with almost the same value of about 10^{-3}. The given Reynolds numbers reach the numerical limits of the code so that the angular momentum transport by the $m = 0$ mode for very large Rm remains an open question, as does its stability toward larger Rm.

Our results do *not* confirm the finding of Lesur & Longaretti (2007) and Longaretti & Lesur (2010), who reported strong dependencies of the normalized angular momentum transport on the microscopic viscosity and/or the basic rotation rate. In particular, we did not find a decay of the angular momentum transport

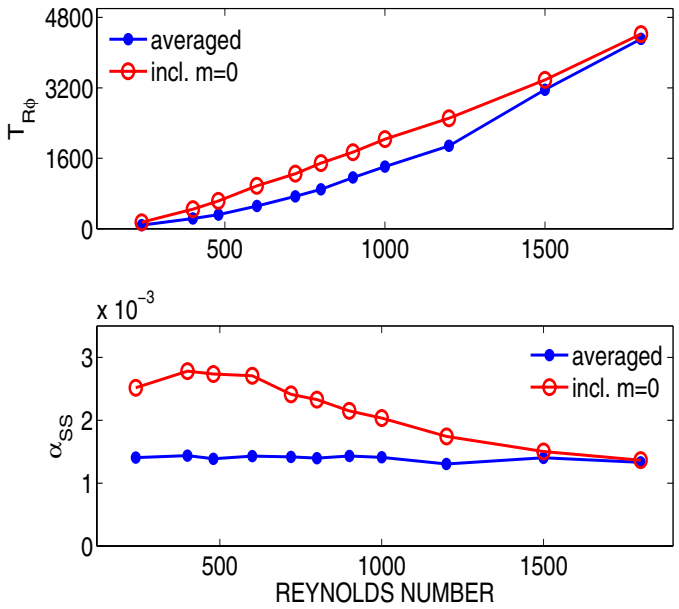

Fig. 12. Same as in Fig. 11 but for S = 30, Pm = 1.

of the MRI for small magnetic Prandtl numbers, in contrast to the conclusions of Fromang et al. (2007). As known from the bifurcation maps of the standard MRI, the actual value of the magnetic Prandtl number is not very important if only the basic rotation and the magnetic background field are normalized without use of the microscopic viscosity. Of course, one can split the Lundquist number in accordance to

$$S = \frac{Rm}{\sqrt{\beta}}, \tag{42}$$

with the plasma $\beta = (\Omega D \sqrt{\mu_0 \rho}/B_z)^2$. But in this case the dependence of α on Rm and β such as described by Longaretti & Lesur (2010) is merely an artificial dependence. According to our findings α_{SS} only depends on the linear product of the magnetic field, the electric conductivity, and the disk size. The total value of α_{SS} does not strongly exceed the limit of 10^{-3}. In comparison with the results of Longaretti & Lesur, the global simulations lead to values lower by one order of magnitude.

8. Discussion

The standard MRI is the instability of differential rotation under the presence of an axial magnetic field. Axisymmetric and nonaxisymmetric modes are excited for supercritical but not too strong fields. One must expect, however, that the nonaxisymmetric modes are quenched by differential rotation that is too strong. On the other hand, the nonaxisymmetric modes are important for any form of hydromagnetic dynamo and/or the evolution of small-scale turbulence and its angular momentum transport. It is this rotational quenching of the nonaxisymmetric modes excited close to the weak-field branch and its consequences for the angular momentum transport that we probed in the present paper.

We have shown by considering a dissipative cylindric TC flow that the MRI only forms nonaxisymmetric modes in a specific domain in the Reynolds number-Lundquist number map. While for large Rm the minimum Lundquist number $S_{MIN} \simeq 1$ for the excitation of axisymmetric modes does not depend on Rm, the minimum magnetic field for the excitation of nonaxisymmetric modes grows for growing Rm. Both the weak-field limit and the strong-field limit of MRI have a positive slope for nonaxisymmetric modes (see Kitchatinov & Rüdiger 2010). The inverse magnetic Mach number Ω_A/Ω_{in} must exceed the value $\simeq 3 \times 10^{-3}$ (for Pm = 1) to obtain excited nonaxisymmetric modes. This quenching effect is very similar for Pm < 1, but it is weaker for Pm > 1 (see Eq. (35)). Fluids with Pm > 1 seem to be favored, therefore, in numerical simulations.

For field amplitudes smaller than the given ones, the standard MRI in cylinders is only formed by axisymmetric rolls, which remained stable in our simulations with Rm up to 10^3. The domain of turbulence, therefore, proved to be (much) smaller than the entire domain of MRI. The most important numerical result of the simulations is that for increasing magnetic Reynolds number the MRI develops from axisymmetric rolls to nonaxisymmetric "turbulence" and returns to axisymmetric rolls. We did not find so far a second bifurcation of the roll instability to more chaotic patterns (Fig. 8).

The dependence of the wave numbers on the field strength is in accordance to the expectation that the axial scales grow for growing fields. Figure 3 shows for $m > 0$ how high values of S correspond to low values of k, which follows from the Taylor-Proudman theorem. The same is true for $m = 0$ but with a specialty: close to the weak-field branch the axial wave length decreases to a minimum for increasing field amplitudes due to the influence of the dissipation. Beginning from this minimum for increasing field amplitudes, the wave lengths grow in accordance to the Taylor-Proudman theorem (see Fig. 4).

The angular momentum transport by the MRI was computed with a nonlinear MHD spectral code which, of course, is able to reproduce all the above given results of the linear theory. In a first step only the angular momentum transport by the nonaxisymmetric modes (which in the model are the only ones to be responsible for turbulence) was computed. Expressed by the MRI-α (38) the results are of a striking simplicity. We did not find an influence of the numerical values of the magnetic Prandtl number and/or the magnetic Reynolds number on the resulting α_{SS} (Fig. 10). The Lundquist number gives the only influence represented by the linear relation (40). The numerical value of the α_{SS} taken at (say) $S \simeq 100$ (1 Gauss for protoplanetary disks at $R = 1$ AU!) is only for the order of 10^{-3}. This value is strongly reminiscent of the numerical results of Brandenburg et al. (1996) obtained with shearing box simulations. Higher values of α_{SS} require stronger fields. Nonlinear relations between α_{SS} and the given axial field component S were not confirmed here.

The inclusion of the angular momentum transport by the axisymmetric "channel" modes only slightly modifies this picture. The maximum amplification of the angular momentum transport by the channel mode is characterized by a factor of two, which for slow rotation gives a stronger increase of the α_{SS} than for fast rotation (Figs. 11 and 12). The total angular momentum transport expressed by α_{SS} due to axisymmetric and nonaxisymmetric modes finally obtains a weak decrease for increasing Reynolds number. There is even indication that for large Reynolds numbers, when the nonaxisymmetric modes eventually become stable, the transport by the axisymmetric modes yields almost the same α_{SS} as the transport by the nonaxisymmetric modes for medium Reynolds numbers.

Acknowledgements. M. Gellert would like to acknowledge support from Deutsche Forschungsgemeinschaft (DFG) within SPP1488.

References

Balbus, S. A., & Hawley, J. F. 1990, BAAS, 22, 1209
Brandenburg, A., & Subramanian, K. 2005, PhR, 417, 1
Brandenburg, A., Nordlund, Å., Stein, R., & Torkelsson, U. 1996, ApJ, 458, 45
Duschl, W. J., Strittmatter, P. A., & Biermann, P. L. 2000, A&A, 357, 1123
Fricke, K. 1969, A&A, 1, 388
Fromang, S., Papaloizou, J., Lesur, G., & Heinemann, T. 2007, A&A, 476, 1123
Gellert, M., Rüdiger, G., & Fournier, A. 2007, Astron. Nachr., 328, 1162
Huré, J.-M., Richard, D., & Zahn, J.-P. 2001, A&A, 367, 1087
Ji, H., Goodman, J., & Kageyama, A. 2001, MNRAS, 325, L1
Kitchatinov, L. L., & Rüdiger, G. 1997, MNRAS, 286, 757
Kitchatinov, L. L., & Rüdiger, G. 2004, A&A, 424, 565
Kitchatinov, L. L., & Rüdiger, G. 2010, A&A, 513, L1
Lesur, G., & Longaretti, P.-Y. 2007, MNRAS, 378, 1471
Longaretti, P.-Y., & Lesur, G. 2010, A&A, 516, A51
Rüdiger, G., & Kitchatinov, L. L. 2005, A&A, 434, 629
Rüdiger, G., & Zhang, Y. 2001, A&A, 378, 302
Rüdiger, G., Schultz, M., & Elstner, D. 2011, A&A, 530, A55
Shalybkov, D., Rüdiger, G., & Schultz, M. 2002, A&A, 395, 339
Stefani, F., Gerbeth, G., Gundrum, T., et al. 2009, Phys. Rev. E, 80, 066303
Velikhov, E. P. 1959, Sov. Phys. JETP, 9, 995